in the presence of C_8V^{2+}, pH 6, and Na_2S, 5×10^{-2} M, as donor, results in the monomer photoproduct, $C_8V^{\bullet+}$, $\phi = 0.2$.[14] When

$$C_8V^{2+} + \beta\text{-CD} \rightleftarrows C_8V^{2+}\cdots\beta\text{-CD} \quad (1)$$

methyl viologen, MV^{2+}, is used as charge relay instead of C_8V^{2+}, substantially lower quantum yields of $MV^{\bullet+}$ are observed. Figure 1b shows the rate of $MV^{\bullet+}$ formation at time intervals of illumination with the TiO_2–β-CD colloid. The quantum yield corresponds to $\phi = 2.6 \times 10^{-4}$ and is 4.4 times lower than that for $C_8V^{\bullet+}$ formation in the analogous system. Similary, the quantum yield for $MV^{\bullet+}$ formation with CdS–β-CD is 3.6 times lower as compared to $C_8V^{\bullet+}$ production. It should be noted that methyl viologen (MV^{2+}) is not associated with β-cyclodextrin.[15] Thus, the high quantum yields for $C_8V^{\bullet+}$ formation in the presence of the β-CD semiconductor stabilized colloids, as compared to that of MV^{2+} photoreduction, is attributed to improved interfacial electron transfer from the excited semiconductor to the relay substrate, C_8V^{2+} (Figure 2). Association of C_8V^{2+} to the β-CD hydrophobic cavity increases the local concentration of the relay in proximity with the semiconductor interface. Consequently, the interfacial electron-transfer rates and reduction of the relay C_8V^{2+} by conduction band electrons are improved. Indeed, the photoreduction process of C_8V^{2+} using the semiconductor–β-CD stabilized colloids is strongly inhibited in the presence of phenol, which associates with the β-CD hydrophobic cavity. Figure 1 (c–e) shows the rate of $C_8V^{\bullet+}$ formation at time intervals of illumination and different concentrations of added phenol. It is evident that the quantum yield for $C_8V^{\bullet+}$ production decreases as the concentration of phenol increases. Thus, phenol that associates to β-CD expels the charge relay C_8V^{2+} from the receptor and consequently the superior configuration for electron transfer is destroyed. Similarly, TiO_2 colloids were stabilized with α-cyclodextrins. The association properties of C_8V^{2+} to α-CD are weaker than those to β-CD ($K_a = 4500$ M^{-1}). Accordingly, the specificity toward C_8V^{2+} photoreduction as compared to MV^{2+} reduction decreases, $\phi(C_8V^{\bullet+})/\phi(MV^{\bullet+}) = 4.0$.

We have compared the photoreduction reactions of C_8V^{2+} and MV^{2+} using TiO_2–β-CD colloids to the similar reactions induced by TiO_2 colloids stabilized by poly(vinyl alcohol), PVA. With TiO_2–PVA colloids the quatnum yield ratio $\phi(C_8V^{\bullet+}):\phi(MV^{\bullet+})$ is 1:1, implying similar efficiencies. With the TiO_2–β-CD colloids the ratio is 4.4:1 and it demonstrates selectivity in the reduction of the C_8V^{2+} relay system.

Laser flash experiments confirm that improved electron transfer occurs to C_8V^{2+} in the presence of TiO_2–β-CD. Flashing the systems that include TiO_2–β-CD and MV^{2+} on C_8V^{2+} at $\lambda = 337.1$ nm results in the formation of $MV^{\bullet+}$ or $C_8V^{\bullet+}$. With MV^{2+} as charge relay, instantaneous accumulation of $MV^{\bullet+}$ is observed that results from electrostatically associated MV^{2+} to the TiO_2–colloid.[5c] With C_8V^{2+} as relay, the instantaneous formation of $C_8V^{\bullet+}$ is followed by a diffusional charge ejection to C_8V^{2+} associated with the β-CD, and the total amount of accumulated $C_8V^{\bullet}$ is ca. 4 times larger than that of $MV^{\bullet+}$.

In conclusion we have stabilized TiO_2 and CdS semiconductor colloids with β-cyclodextrins. The tailored semiconductor–receptor configuration and proper design of the charge relay provide means to control interfacial electron transfer and introduce selectivity in the reduction of relay substrates. The association of the relay to the receptor sites increases the local concentration of the relay at the colloid interface and consequently improves the interfacial electron-transfer process. Further applications of semiconductor–receptor colloids could be envisaged. These include effective and selective charge injection via the selective association of chromophores to β-CD or selective synthesis through immobilization of catalysts on the semiconductor sites. These aspects are now being examined in our laboratory.

Acknowledgment. The support of the Singer Foundation is gratefully acknowledged.

(14) Light intensity was determined by using Reinecke's salt actinometry. cf.: Wanger, E. E.; Adamsonn, A. W. *J. Am. Chem. Soc.* **1966**, *88*, 394.
(15) Matsue, T.; Kato, T.; Akiba, U.; Osa, T. *Chem. Lett.* **1985**, 1825.

Spectroscopic and Structural Evidence of Temperature Dependent Charge Localization and Structural Differentiation of the Fe Sites within the $[Fe_6S_6X_6]^{2-}$ Clusters (X = Cl, Br)

D. Coucouvanis,* M. G. Kanatzidis, A. Salifoglou, and W. R. Dunham

Department of Chemistry, University of Michigan Ann Arbor, Michigan 48109

A. Simopoulos, J. R. Sams,[1] V. Papaefthymiou, and A. Kostikas

Nuclear Research Center Demokritos Aghia Paraskevi, Attiki, Greece

C. E. Strouse

Department of Chemistry and Biochemistry and the Solid State Science Center, University of California Los Angeles, California 90024

Received May 8, 1987

The recently reported $[Fe_6S_6L_6]^{3-}$ clusters[2] are new members in the general series of the synthetic Fe/S clusters that contain the $[Fe_2S_2]_n^{n+}$ cores. They are metastable species and thermally or catalytically can be converted quantitatively to the $[Fe_4S_4X_4]^{2-}$ "cubanes" (eq 1).

$$2[Fe_6S_6X_6]^{3-} \rightarrow 3[Fe_4S_4X_4]^{2-} \quad (1)$$

The oxidized, $[Fe_6S_6X_6]^{2-}$, prismane clusters can be obtained in nearly quantitative yields by chemical oxidation of the $[Fe_4S_4X_4]^{2-}$ clusters[2c] (eq 2) (X = Cl, Br) with $[(C_5H_5)_2Fe]^+[PF_6^-]$.

$$3[Fe_4S_4X_4]^{2-} + 2[Fe(C_5H_5)_2]^+ \rightarrow 2[Fe_6S_6X_6]^{2-} + 2Fe(C_5H_5)_2 \quad (2)$$

The Mossbauer spectra of the $[Fe_6S_6X_6]^{2-}$ clusters for X = Cl, I [or Br, II], were examined at various temperatures in the range from 1.6 K to ambient temperature (AT). The spectra (Figure 1) generally show two broad lines of unequal intensities at temperatures above 100 K. The average values of the isomer shift (IS) and quadrupole splitting (Δ_{Eq}) for these doublets above 100 K are 0.44 (1), 0.62 (1) and 0.44 (1), 0.70 (1) mm/s, respectively, for I and II. These values, which represent iron atoms in a formal +2.66 oxidation state, as expected, are somewhat smaller than corresponding values for the $[Fe_6S_6X_6]^{3-}$ clusters, which contain iron atoms in a +2.5 formal oxidation state.[2b] For the latter, IS and Δ_{Eq} values of 0.52 (1) and 0.95 (1) mm/s for X = Cl and 0.54 (1) and 1.00 (1) mm/s for X = Br have been observed at 125 K. At 1.6 K the high velocity line clearly shows partially resolved structure that suggests at least three peaks. The structure persists to about 50 K and gradually becomes obscure at higher temperatures. The spectra for both I and II at 4.2 K were fitted by the superposition of three symmetric quadrupole doublets constrained to equal intensities and line widths. This model implies the grouping of the iron ions into three pairs characterized by different IS and Δ_{Eq} values with the irons within each pair being equivalent. Two realistic combinations of six peaks into quadrupole doublets can be chosen.[3] For combination (a) in the low tem-

(1) On leave of absence, Chemistry Department, University of British Columbia, Vancouver, British Columbia, Canada.
(2) (a) Kanatzidis, M. G.; Dunham, W. R.; Hagen, W. R.; Coucouvanis, D. *J. Chem. Soc., Chem. Commun.* **1984**, 356. (b) Kanatzidis, M. G.; Hagen, W. R.; Dunham, W. R.; Lester, R. K.; Coucouvanis, D. *J. Am. Chem. Soc.* **1985**, *107*, 953. (c) Coucouvanis, D.; Kanatzidis, M. G.; Dunham, W. R.; Hagen, W. R. *J. Am. Chem. Soc.* **1984**, *106*, 7998. (d) Kanatzidis, M. G.; Salifoglou, A.; Coucouvanis, D. *J. Am. Chem. Soc.* **1985**, *107*, 3358. (e) Kanatzidis, M. G.; Salifoglou, A.; Coucouvanis, D. *Inorg. Chem.* **1986**, *25*, 2460.

0002-7863/87/1509-6863$01.50/0

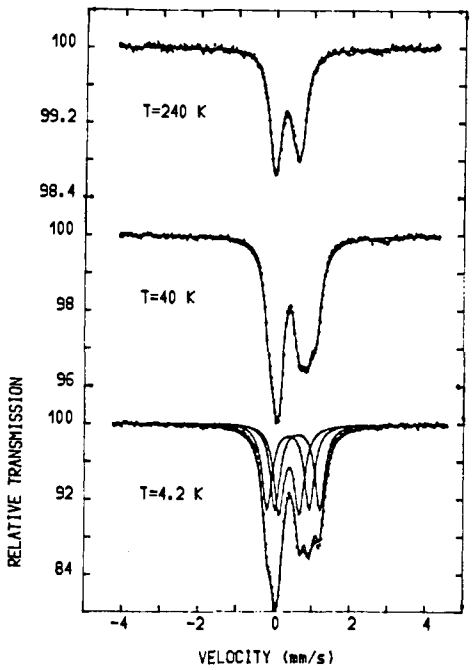

Figure 1. Mossbauer spectra at 4.2, 40, and 240 K of I. The solid lines are simulated spectra calculated with the parameters given in the text.

perature limit (for I), two quadrupole doublets that correspond to four of the iron sites are characterized by an IS of 0.36 (1) and 0.39 (1) mm/s. The remaining two iron sites give rise to the third quadrupole doublet with an IS of 0.68 mm/s. The Δ_{Eq} values for the three doublets are 0.64 (1), 1.12 (1), and 1.09 (1) mm/s, respectively. The temperature variation of the IS and Δ_{Eq} values for combination (a) is very similar to the one reported for certain FeOCl intercalation compounds.[4]

For combination (b) at 4.2 K, the spectra can be interpreted in terms of two iron sites with an IS of ~0.41 mm/s and four sites with IS values 0.53 (1) and 0.49 (1) mm/s. Associated with these three doublets are Δ_{Eq} values of 0.54, 1.40 (1), and 0.91 (1) mm/s, respectively. The temperature variation of the IS values in combination (b) follows closely the one expected from the second-order Doppler, SOD, shift effect; however, the variation of the Δ_{Eq} values with temperature is quite pronounced. Indeed the observed behavior of Δ_{Eq} is rather inconsistent with the symmetry of the iron sites in the molecule and the assigned valences on the basis of the IS values.

The possibility that structural changes may have been responsible for this apparent charge localization in I and II[5] was considered, and the structure of I was determined[6] at ~144 K and at ~20 K. The results are similar to those obtained in the initial[2c] (298 K) structure determination of I. The differences between the 298 and 144 K structures are insignificant, and both determinations indicate essentially equivalent iron sites. In the higher temperatures, 298 K [144 K], the mean values[7] for the three Fe–S bonds around each iron are within 3σ and range between 2.256 (3) Å [2.256 (7) Å] for Fe(1) to 2.270 (2) Å [2.275 (4) Å] for Fe(2). The mean value of all 18 Fe–S bond lengths is 2.265 (2) Å [2.266 (4) Å]. These values also are very close to the Fe–S bond, for all irons, obtained in the 298 K structure of II at 2.262 (8) Å.

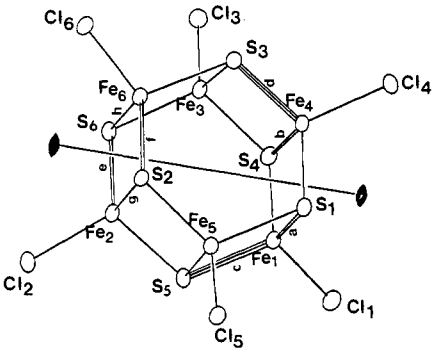

Figure 2. Structure and labeling of the $[Fe_6S_6Cl_6]^{2-}$ anion. Thermal ellipsoids as drawn by ORTEP (Johnson, C. K. ORNL-3794; Oak Ridge National Laboratory: Oak Ridge, TN, 1965) represent the 50% probability surfaces. The twofold axis shown in the figure is idealized and not crystallographically required (see text for details). The labeled Fe–S bonds at 298, 144, and 20 K, respectively, have the following values (Å): (a) 2.262 (2), 2.257 (2), 2.250 (3); (b) 2.272 (2), 2.268 (2), 2.253 (3); (c) 2.253 (2), 2.243 (2), 2.225 (3); (d) 2.259 (2), 2.249 (2) 2.222 (3); (e) 2.268 (2), 2.266 (2), 2.251 (3); (f) 2.253 (2), 2.247 (2), 2.242 (3); (g) 2.253 (2), 2.268 (2), 2.298 (3); (h) 2.277 (2), 2.288 (2), 2.307 (3). A complete table that lists the monotonic changes in the structural parameters of I as a function of temperature has been deposited.

The 20 K structure shows (Figure 2) a remarkable divergence in the Fe–S bond lengths. The approach to this divergence is evident in the monotonic changes of the Fe–S bond lengths as a function of temperature. The Fe–S bond lengths in I appear to be related by a noncrystallographic twofold axis (Figure 2) that separates the iron atoms into three pairs. The distortion that the Fe_6S_6 core has undergone at 20 K consists of a slight elongation about the idealized twofold axis shown in Figure 2. The effects of this elongation also are apparent in small but systematic angular changes within the hexagonal faces of the Fe_6S_6 core.

The pattern of Fe–Fe distances at 20 K also reflects the twofold symmetry of the distortion with short Fe(2)–Fe(5) and Fe(3)–Fe(6) distances (ca. 2.71 Å), intermediate length Fe(1)–Fe(5) and Fe(3)–Fe(4) distances (ca. 2.76 Å), and long Fe(1)–Fe(4) and Fe(2)–Fe(6) distances (ca. 2.81 Å). To the extent that the highest occupied molecular orbitals of this complex are predominantly Fe in character,[2c] the pattern of Fe–S bonding observed may just be a consequence of an instability of the Fe_6 framework which produces an asymmetric localization of charge. It is noteworthy that although the Fe–Cl bond lengths in the cluster show significant variation they do not reflect the same twofold symmetry as the Fe–S and Fe–Fe distances. The variation in the Fe–Cl distances almost certainly results from asymmetric lattice interactions. This asymmetry is presumably responsible for stabilizing the observed conformer with respect to the two threefold related alternatives.

In some respects the core instability observed in the $[Fe_6S_6Cl_6]^{2-}$ cluster is analogous to that observed for the $[Fe_4S_4L_4]^{2-}$ clusters[8] (L = Cl; SC_6H_5). In the latter the D_{2d} distortion in the cubane structure results in the appearance of two long and four short Fe–Fe bonds but leaves the four ion atoms equivalent. In the prismane case the C_2 distortion gives three different Fe–Fe distances and three chemically distinct iron sites. The Mossbauer spectra of the $(Ph_3P)_2N^+$ salt of I in the solid state *and in frozen* $C_2H_4Cl_2$ *solution* at 4.2 K show partially resolved structure es-

(3) The fit determines the positions of six Lorentzian lines of equal intensities and line widths that may be combined in six different ways into three quadrupole doublets. The choice of the physically meaningful among them may be made on the basis of the values of the IS. The latter, for tetrahedral FeS_4 coordination, varies between ~0.33 mm/s for Fe^{3+} to ~0.65 mm/s for Fe^{2+}.

(4) Herber, R. H.; Eckert, H. *Phys. Rev. B* **1985**, *31*, 34. In this paper the application of a time dependent exchange perturbation model has been successfully employed in reproducing an unusual temperature behavior of the IS and a sigmoidal temperature variation of the quadrupole splitting.

(5) The Mossbauer spectra of II also can be analyzed in terms of two combinations of doublets: combination (a) IS values 0.38 (1), 0.40 (1), 0.64 (1) mm/s; Δ_{Eq} values 0.69 (1), 1.18 (1), 1.10 (1) mm/s. Combination (b) IS values 0.51 (1), 0.50 (1), 0.41 (1) mm/s; Δ_{Eq} values 0.95 (1), 1.38 (1), 0.64 (1) mm/s.

(6) Crystal and refinement data for I at 144 K (University of Michigan) at 20 K (University of California, Los Angeles) and for II at 298 K have been deposited. The structural data for I at 144 and 20 K were obtained from the same crystal.

(7) For the mean values, the entries in parentheses represent the larger of the standard deviations for an individual value estimated from the inverse matrix or of the standard deviation $\sigma = [\Sigma(x_i - x)^2/N(N-1)]^{1/2}$.

(8) Berg, J. M.; Holm, R. H. In *Iron-Sulfur Proteins*; Spiro, T., Ed.; Wiley: New York, 1983; Vol. IV, p 27 and references therein.

sentially identical with that observed for I (Figure 1). It appears therefore that the C_2 distortion, evident in the 20 K structure of I, is an intrinsic structural characteristic of the $[Fe_6S_6Cl_6]^{2-}$ anion, and lattice effects are not the cause of the observed distortions in the $[Fe_6S_6]^{4+}$ core. This work represents another case in which caution must be exercised in the association of spectroscopic data obtained at cryogenic temperatures with structure and function characteristics obtained at ambient temperatures.

Acknowledgment. We acknowledge the generous support of this research by a grant from the National Institutes of Health, D.C. (GM-26671) and C.E.S. (GM-35329-02)

Supplementary Material Available: Tables of crystal and refinement data, positional and thermal parameters, and intramolecular distances from the 20 K structure (9 pages); listing of observed and calculated structure factors for $Fe_6S_6Cl_6^{2-}$ (24 pages). Ordering information is given on any current masthead page.

Disilaoxiranes: Synthesis and Crystal Structure

Howard B. Yokelson, Anthony J. Millevolte, Gregory R. Gillette, and Robert West*

Department of Chemistry
University of Wisconsin—Madison
Madison, Wisconsin 53706

Received June 25, 1987

Since the discovery of the first stable disilenes in 1981,[1] studies on the reactivity of the silicon–silicon double bond have revealed a rich and diverse chemistry.[2] It is now well established that the disilenes **1** react readily with triplet oxygen either in solution or

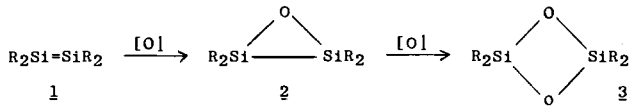

(a) R = Mes = 2,4,6-trimethylphenyl

(b) R = Xyl = 2,6-dimethylphenyl

(c) R = Dmt = 2,6-dimethyl-4-tert-butylphenyl

the solid state to give the 1,3-cyclodisiloxanes **3**.[3] A monooxygenated adduct, the disilaoxirane **2**, was identified as a minor product in the low-temperature oxidation of (*E*)-1,2-dimesityl-1,2-di-*tert*-butyldisilene.[4] We now report the synthesis of several tetraaryldisilaoxiranes, prepared by the reaction of tetraaryldisilenes **1a–c** with dinitrogen oxide as well as the molecular structure of tetramesityldisilaoxirane, **2a**.

When a stream of dinitrogen oxide was bubbled through a bright yellow solution of disilene **1a** in benzene at room temperature, the solution decolorized slowly. Only a single new resonance (δ −27.2) was observed in the silicon-29 spectrum of the reaction mixture. Crystals of the benzene solvate of **2a** ($C_{36}H_{44}Si_2O{\cdot}C_6D_6$, m = 633.0) suitable for X-ray crystallographic

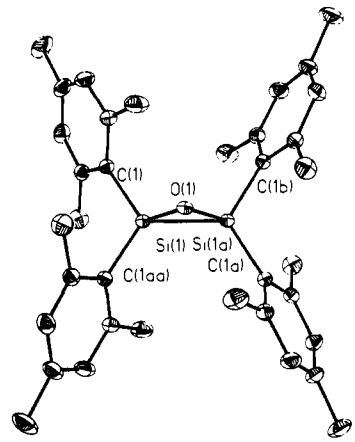

Figure 1. Molecular structure of **2a**. (Hydrogens omitted for clarity.) Bond lengths (pm) are as follows: Si(1)–Si(1a), 222.7 (2); Si(1)–C(1), 187.8 (2); Si(1)–O(1), 173.3(3). Bond angles (deg) are as follows: Si(1)–Si(1a)–O(1), 50.0 (1); Si(1)–O(1)–Si(1a); 80.0 (2).

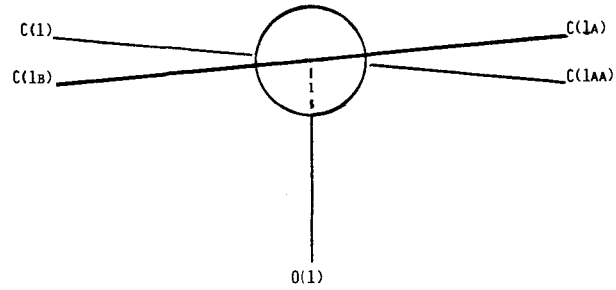

Figure 2. Newman projection of **2a** along the Si–Si axis showing the twist angle. The numbering scheme is shown in Figure 1; Si(1) is in the back of Si(1a).

analysis were obtained from this reaction mixture on standing.[5] Disilaoxirane **2a** is inert to further oxidation by dinitrogen oxide, even when heated in benzene solution at 80 °C for several days. However, on exposure to air **2a** undergoes further oxidation to the cyclodisiloxane **3a** with a half-life in solution of several hours at 20 °C. As was noted for their disilene precursors, the air stability of the disilaoxiranes is greatly enhanced in the solid state.

The X-ray crystal structure of **2a** was solved by direct methods and refined by blocked-cascade least-squares refinement[6] based on F with use of 1801 data with $F_o > 3\sigma(F_o)$. Final discrepancy indices are R1 = 0.060, R2 = 0.069, GOOF = 1.71.[7] Figure 1 shows an ORTEP diagram of **2a**. The molecule possesses a twofold rotation axis which passes through the oxygen and bisects the silicon–silicon bond. It is remarkable that the silicon and the carbon atoms directly attached to each silicon are coplanar. That is, the sum of the bond angles C–Si–Si′, C′–Si–Si′, C–Si–C′ about each silicon atom is 360°. The torsional distortion along the silicon–silicon axis results in a twist angle of 10°, as illustrated

(1) (a) West, R.; Fink, M. J.; Michl, J. *Science* (Washington, D.C.) **1981**, *214*, 1343. (b) Masamune, S.; Hanzawa, Y.; Murakami, S.; Bally, T.; Blount, J. *J. Am. Chem. Soc.* **1982**, *104*, 1150.

(2) For reviews of disilenes, see: (a) West, R. *Angew. Chem.* **1987**, in press. (b) Raabe, G.; Michl, J. *Chem. Rev.* **1985**, *85*, 419–509. (c) West, R. *Pure Appl. Chem.* **1984**, *56*, 163–173.

(3) (a) Fink, M. J.; De Young, D. J.; West, R.; Michl, J. *J. Am. Chem. Soc.* **1983**, *105*, 1070–1071. (b) Fink, M. J.; Haller, K. J.; West, R.; Michl, J. *J. Am. Chem. Soc.* **1984**, *106*, 822–823. (c) Michalczyk, M. J.; Fink, M. J.; Haller, K. J.; West, R.; Michl, J. *Organometallics* **1986**, *5*, 531–538.

(4) (a) Michalczyk, M. J.; West, R.; Michl, J. *J. Chem. Soc. Chem. Commun.* **1984**, 1525–1526. (b) The formation of a tetraalkyldisilaoxirane has been proposed as a reactive intermediate in the photolysis of hexaneopentyltrisilaoxetane, see: Watanabe, H.; Tabei, E.; Goto, M.; Nagai, Y. *Ibid.* **1987**, 522–523.

(5) For compund **2a**: mp 187–190 °C; ^{1}H (270 MHz, C_6D_6) δ 2.02 (s, 12 H), 2.56 (s, 24 H), 6.61 (s, 8 H); ($CDCl_3$) δ 2.21 (s, 12 H), 2.31 (s, 24 H), 6.68 (s, 8 H); ^{29}Si NMR (71.5 MHz, C_6D_6) δ −26.92; IR (KBr, cm^{-1}) 3000, 1610, 1460, 1275, 1070, 1020; UV (THF) λ_{max} 235, 293, 341 (sh); mass spectrum (30 eV) calcd for $C_{36}H_{44}Si_2O$ m/e 548.2931, found m/e 548.2930.

(6) SHELXTL, Nicolet X-ray Instruments, Madison WI, 1985.

(7) (a) Four molecules of **2a** and four molecules of benzene-d_6 crystallize in the orthorhombic space group (*Ccca*) with cell dimensions as follows: a = 12.181 (2) Å, b = 19.736 (4) Å, c = 14.671 (3) Å, (T = 150 ± 2 K), λ(Mo Kα) = 0.71073 Å; V = 3046.2 Å^3, D(calcd) = 1.21 g/cm^3, and Z = 4. Each molecule is required to possess crystallographic symmetry, and **2a** is located on a 222 site at (0 $^1/_4$ $^3/_4$) with the Si–Si bond along one twofold axis, and the bridging oxygen atom on one of the twofold axes perpendicular to the Si–Si bond axis. Thus there are two positions for the oxygen atom, and refinement of the occupancy factor for the oxygen atom showed the unique portion to be $^1/_4$ occupied, confirming the oxygen to silicon ratio in the unit cell is 1:2; subsequently this occupancy factor was fixed at 0.25. Each of the (ordered) benzene molecules is located on a 222 site. (b) Tables of the final atomic coordinates, anisotropic thermal parameters, and selected distances and angles are given as Supplementary Material.

0002-7863/87/1509-6865$01.50/0